Electrochemical and Solid-State Letters, **8** (11) A592-A595 (2005)
1099-0062/2005/8(11)/A592/4/$7.00 © The Electrochemical Society, Inc.

Characteristic Thickness for a Dense $La_{0.8}Sr_{0.2}MnO_3$ Electrode

Erik Koep, David S. Mebane, Rupak Das, Charles Compson,* and Meilin Liu,z**

School of Materials Science an Engineering, Georgia Institute of Technology, Atlanta, Georgia 30332-0245, USA

Dense $La_{0.8}Sr_{0.2}MnO_3$ (LSM) electrodes were patterned by photolithography and fabricated via pulsed-laser deposition on Y_2O_3-stabalized ZrO_2 (YSZ) electrolytes. Impedance analysis shows that the interfacial polarization resistance decreases significantly as electrode thickness drops below a critical value, beyond which the top surface of the LSM becomes active for oxygen reduction. However, when the LSM electrodes become too thin, the in-plane sheet resistance of the LSM starts to limit the utilization of the electrodes along their length. Quantification of the characteristic thickness is important not only to intelligent design of practical mixed-conducting electrodes but also to electrode design for fundamental studies.
 [DOI: 10.1149/1.2050607]

Manuscript submitted May 18, 2005; revised manuscript received June 28, 2005. Available electronically September 12, 2005.

Due to its favorable catalytic properties and chemical compatibility with Y_2O_3-stabalized ZrO_2 (YSZ), Sr-doped $LaMnO_3$ (LSM) has become a popular material choice for solid oxide fuel cell (SOFC) cathodes.[1-3] Although often treated as a pure electronic conductor, LSM has been shown to exhibit some, albeit very low, ionic conductivity.[4] In fact, when a dense LSM electrode is sufficiently thin, it behaves more like a mixed ionic/electronic conductor (MIEC) than a pure electronic conductor. In general, the oxygen reduction reaction may occur via three distinct pathways for an MIEC such as LSM:[5]

1. Direct electrochemical reduction of oxygen may occur at the three-phase boundary (TPB), where oxygen is available in the gaseous phase.
2. A surface adsorption step has been proposed in which oxygen may be adsorbed and partially reduced before moving along the electrode or electrolyte surface to the TPB, leading to a finite width of the TPB.
3. Incorporation of oxygen into the electrode through the MIEC surface may occur with subsequent transport of oxygen ions through the electrode bulk to the electrolyte.

Clearly, the rate of oxygen reduction through pathway 3 depends critically on the transport properties and thickness of the dense LSM layer. As the LSM electrode becomes thinner, the resistance of pathway 3 drops and, if bulk transport for this mechanism is rate-limiting, the rate of oxygen reduction at the surface will increase.

While there is little argument about the possible pathways, debate abounds regarding the individual contributions of each. Many researchers have found the interfacial polarization resistance to be proportional to the amount of available three-phase boundary (L_{tpb}),[6-10] whereas others have found that electrode performance depends more on bulk transport phenomena.[11-15] For instance, the effective utilization of dense MIEC electrodes is most likely determined by the rate of ionic transport through the MIEC electrode.[16,17] In general, all possible reaction paths should be considered, although some paths may become more important than others under certain conditions.

In reality, the operating conditions and electrode geometry may very well define the dominant reaction pathway. Specifically, it has been suggested that the highly porous electrodes most common in SOFC fabrication may not take full advantage of the ionic properties of the material.[18] Furthermore, simple extension of TPB length may not be the most effective approach to reducing the interfacial polarization resistance.[19] It becomes clear, then, that the best method for analysis of these three competing effects is to compare all three simultaneously in a controlled manner. As limiting cases, studies on porous MIEC electrodes may feature the contributions of the TPB while studies on dense MIEC electrodes (with essentially no TPB length) reflect the effect of bulk transport properties. To compare the relative contribution of each pathway, properly designed patterned electrodes of LSM (with a clearly defined, nonzero TPB length) should be employed. In such an experiment the competing mechanisms can be quantitatively evaluated. While several previous studies with patterned microelectrodes have clearly demonstrated the effect of TPB length on the performance of microelectrodes, the characteristic thicknesses of various MIEC electrodes are yet to be quantified.[8,10,11,20-26] Here, we report the effect of dense LSM electrode thickness on the utilization of patterned microelectrodes and a critical thickness below which the LSM surfaces become active and make significant contributions to oxygen reduction. Also quantified is another critical thickness at which the in-plane sheet resistance becomes significant.

Experimental

YSZ pellets prepared by tape casting were used as the substrates for patterned electrode and reference electrode deposition. Daiichi YSZ powder, with a mean particle size of 0.26 μm, was suspended in a solvent-based slurry using menhaden fish oil (dispersant) polyvinyl butyral (binder), polyethylene glycol (type I plasticizer) and butyl benzyl phthalate (type II plasticizer). The slurry was prepared in a two-stage process and ballmilled for at least 24 h between stages using 7 mm YSZ charge. Prior to casting, the slurry was de-aired by placing the jar in a vacuum chamber for about 5 min at −10 in. Hg.

A stationary blade six-foot tabletop caster from Richard E. Mistler Inc. was used to cast the slurry at a blade height of ~150 μm. The tabletop caster was equipped with a dc motor, variable speed control, heated five-foot casting bed, one-foot square granite casting block, and counterdirectional mass-controlled airflow. The cast tape was then cut into 1.7 cm disks and laminated into stacks of three using a uniaxial press. Semi-constrained firing techniques were used in order to minimize warpage while allowing the tape to sinter without cracking. The fired pellets experienced about 22% total shrinkage during firing as determined by dilatometry, were ~400 μm thick according to scanning electron microscopy (SEM), and attained 95% of theoretical density as measured by the Archimedes method.

To minimize the impact of impurities contaminating the film, all cleaning and photolithographic processes have been performed in a class 10 cleanroom. Once inside the cleanroom, the YSZ electrolyte was cleaned in subsequent baths of acetone, ethanol, and deionized water, then dried with compressed nitrogen.

A lift-off process utilizing a bilayer resist was developed prior to film deposition. The details of the photolithography process have been reported elsewhere.[27] Following pulsed laser deposition (PLD), the negative photoresist pattern was removed leaving only the desired pattern and thickness. Electrode thickness was controlled by deposition time and verified by profilometry.

The thin films were prepared via a PLD method. Specifically, the target was encapsulated in a high-vacuum chamber pumped to a

* Electrochemical Society Student Member.
** Electrochemical Society Active Member.
z E-mail: meilin.liu@mse.gatech.edu

base pressure of 1×10^{-4} Torr. A COMPex model 205 laser from Lambda Physik with a 25 ns pulse duration was used for ablation. It was operated at 10 Hz and 353 mJ yielding a typical deposition rate around 2 Å/s.

The single-phase $La_{0.8}Sr_{0.2}MnO_3$ target was prepared by solid-state sintering method. LSM powder was synthesized from a molar ratio of La_2O_3, $SrCO_3$, and Mn_2O_3. The powder mixture was ball-milled, pressed isostatically to a pressure of 11 tons and calcined at 1150°C for 5 h. The pellet was then ground and ballmilled again to a fine powder. The powder was repressed into a pellet and sintered into its final shape at 1300°C for 5 h.

The working electrodes consisted of a patterned electrode covering an area of 0.6×0.6 cm with an adjacent reference electrode. The electrode array consisted of 60 patterned rectangular electrodes 40 μm in width separated by 60 μm gaps. A platinum current collector was lithographically patterned and deposited on top of the working electrode. The current collector consisted of 12 identical 50 μm wide platinum strips separated by exactly 490 μm. All 12 platinum strips connected to a platinum pad in order to facilitate wire attach. The adjacent reference electrode was a 0.2×0.5 mm platinum rectangle separated from the working electrode by less than 20 μm. A painted silver electrode (Hereaus C8800SD) was used on the opposite side of the electrolyte as a counter electrode. Cells were then placed in a tube furnace for impedance measurement. Each sample was run individually at constant temperature in 50°C increments ranging from 500 to 750°C. A Solatron 1255 frequency response analyzer connected through a Solatron 1287 electrochemical interface collected impedance data over a range from 100 kHz to 0.01 Hz using both two and three-electrode configurations.

PLD of lanthanum containing oxides has been shown to provide stoichiometric thin films under high-vacuum conditions with minimal requirements for postdeposition anneal steps.[16] Excess oxygen has been shown to create nonuniform films with significant degrees of surface roughness. Leakage current and fatigue were also found to decrease with oxygen partial pressure.[28,29] Furthermore, thin layers of LSM deposited via PLD were affected by the crystallographic orientation of the substrate.[30] To ensure a smooth and uniform surface, PLD was performed under high vacuum with postdeposition SEM analysis. By depositing the films directly onto a polycrystalline substrate, the preferred tetragonal phase and stoichiometry was maintained during laser ablation, as confirmed by X-ray analysis (Panalytical X-pert Pro MPD diffractometer).[31]

Results and Discussion

SEM analyses confirm that the LSM electrodes are thin, dense, and relatively defect-free. Furthermore, the actual thickness and TPB length are as calculated. An SEM presented in Fig. 1 demonstrates close control of the electrode geometry throughout the array.

Shown in Fig. 2 are some typical impedance spectra of the interfacial resistance between the electrolyte and the patterned LSM microelectrode. In this case, the impedance contribution from the electrolyte/counter electrode interface can be neglected since it accounts for less than 1% of the total interfacial polarization resistance. The interfacial resistances were readily extracted through comparison of multiple configurations of two and three electrode measurements. Due to the use of a reference electrode, the cathode/electrolyte interfacial polarization resistance can be taken from the intercepts of the impedance curve on the real axis. The impedance data clearly indicate that the thickness of dense electrodes plays a significant role in the overall performance. Furthermore, the impedance data show the importance of simultaneous transport of electronic and ionic defects through the bulk phase of LSM. Because all of the electrodes were patterned with approximately the same amount of surface area and TPB length, any significant differences in behavior must be related to the geometric thickness of electrode. Furthermore, because the electrode of lowest interfacial resistance is not the thinnest electrode, it appears that there is a performance-related minimum thickness for dense LSM electrodes.

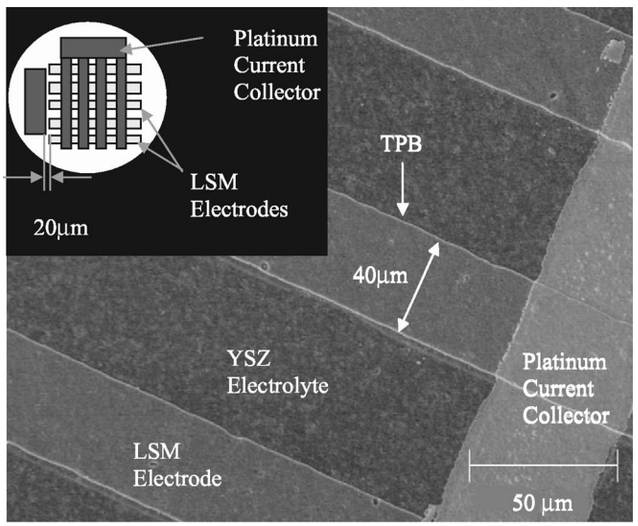

Figure 1. An SEM of LSM patterned electrodes (with constant TPB length and surface area) on a YSZ substrate The width of the LSM strip is 40 μm and the gap between two adjacent strips is 60 μm. Platinum current collector strips run perpendicular to the LSM strips. A schematic of the cell is provided in the inset.

Figure 3 displays the dependence of the interfacial impedance on the electrode strip thickness at 700 and 750°C. Several unique traits are evident for each temperature range. In particular, note the peak conductance, located between 0.18 and 0.22 μm, followed by a rapid decay with increasing thickness. It should also be noted that the high-thickness decay behavior appears to asymptotically approach a nonzero value. This value, approximately 0.0059 Ω^{-1} at 700°C, has been attributed to the standardized factors within the cell. Among these are the TPB and surface transport contributions of the LSM array as well as the catalytic contributions of the platinum current collector. Because these factors have been systematically controlled through the design and fabrication stages, their contributions should be constant over the entire range of electrode thickness. Consequently, this background value can be subtracted from the overall conductance to yield the contribution from a pathway depending upon bulk transport through the dense MIEC.

Because only the rate of the oxygen reduction process that involves bulk transport depends upon electrode thickness, the dramatic reduction in electrode performance with increasing thickness must be due to the increased resistance to bulk transport of ionic

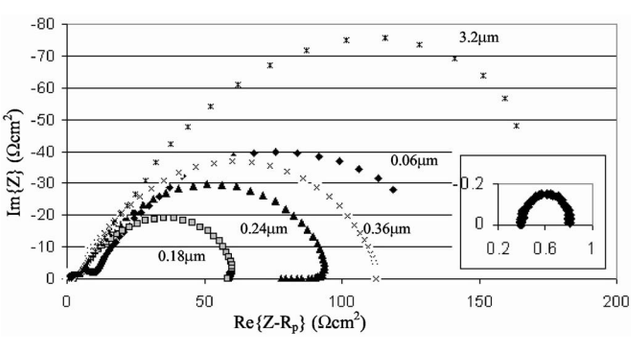

Figure 2. Typical impedance spectra for an interface between the electrolyte and the patterned electrodes (working electrode) of constant TPB length and surface area with varying thickness at 700°C. The inset in the bottom right corner shows a typical impedance spectrum for the counter electrode-electrolyte interface, implying that it is less than 1% of that for the working electrode-electrolyte interface.

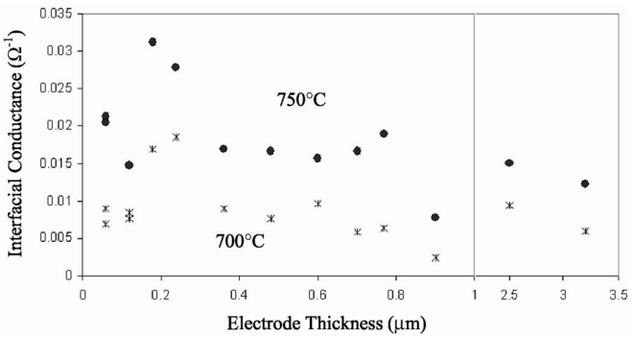

Figure 3. Plot of $1/R_p$ vs electrode thickness. The horizontal axis has been compressed in some regions to accommodate the scope of all the tested electrodes.

defects. In fact, for 700°C the overall conductance drops below 26% of its peak value by 0.36 μm in thickness. This thickness value is important since it is where the interfacial polarization resistance first drops below 1/e, or ~37%. While 1/e is a somewhat arbitrary selection, this value is commonly used as a characteristic value for many physical phenomena (e.g., relaxation time and diffusion length). In defining the characteristic thickness of a material by the 1/e value, a quantitative value can be assigned to each material to allow easy comparison. This critical thickness can be viewed as the thickness below which the mixed conducting behavior of the electrode can no longer be neglected.

Further reductions in the electrode thickness facilitate transport through the bulk phase of the MIEC, catalytically activating the top surface of the pattern and thus improving electrode performance. Because ionic transport is thermally activated, the characteristic bulk-active thickness can be expected to vary with temperature. The characteristic thickness has been plotted as a function of temperature on the insert in Fig. 4. As expected, a downward linear trend can be discerned with decreasing temperature.

One final point of interest in Fig. 3 is the dramatic drop in electrode performance at 0.12 μm thickness. It is believed that this drop-off in performance is due primarily to limitations of current collection. Below 0.18 μm, the sheet resistance within the patterned electrode climbs to values high enough such that the entire surface area of the patterned electrode may no longer be assumed to be at a constant overpotential. At this point, many parts of the electrode array, particularly those locations far from the current collector strips, become less active. The further away that a cathode surface

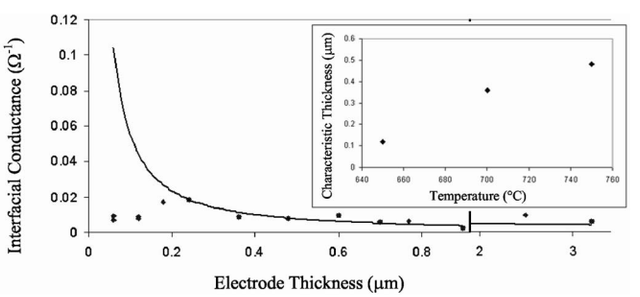

Figure 4. Plot of $1/R_p$ vs electrode thickness at 700°C. The horizontal axis has been compressed in some regions to accommodate the scope of all the tested electrodes. Points indicate the experimental values while the solid curve is the corrective model. The insert in the top right corner is a plot of Characteristic thickness as a function of temperature for LSM. A downward linear trend can be discerned with decreasing temperature.

element is from the current collector, the less it will contribute to the overall electrode performance, leading to larger interfacial resistances.

Because the electrode geometry is very well known, a computational model of sheet resistance was developed to predict the effect of sheet resistance on electrode performance. The details of this model have been reported elsewhere.[32] From the model, the total percentage of the cathode array utilized, defined as the percent utilization, was estimated for a given geometry. For the thicker electrodes, the percent utilization was nearly 100% and changed very little. However, when applied to the films of 0.18, 0.12, and 0.06 μm in height, the percent utilization dropped dramatically from 76.96 to 52.64, and 30.64%, respectively. The cumulative effect of a drop in utilization is displayed graphically in Fig. 4. Specifically, in this figure all interfacial conductance values have been normalized to 100% utilization and replotted against the original values. From the shape of the corrected value curve further reductions in electrode thickness should yield dramatic increases in electrode performance.

The percentage utilization figures demonstrate the effect of the overall sheet resistance and explain the interfacial phenomena for very thin films. Although the electrochemical performance of the 0.06 μm thick electrode should be the best due to facile ionic diffusion, with only roughly 30% of the cathode material utilized, the performance fell far short of expectations. Inefficient injection of electrons from the current collector to the LSM electrode strips is the cause of this behavior. Though the relatively high electronic conductivity of LSM is often cited as the material's primary advantage,[33] the results presented here indicate that the electronic conductivity may be the limiting factor in the case of thin films.

The implication of these size limits impacts the rational design of LSM electrodes. On one hand, small grains have the large amounts of surface area necessary for oxygen reduction. On the other hand, current collection limitations may reduce the effective utilization for very small particles. The critical thickness value of 0.36 μm provides an upper limit to the effective thickness of LSM particles. The lower limit will be determined by the geometry and current collection methods of the system.

Conclusions

This study has demonstrated the effect of electrode thickness on the performance of dense LSM electrodes. Although LSM is often regarded as a pure electronic conductor, this study has shown that for very thin electrodes, the mixed ionic/electronic conducting behavior of LSM can be significant.

The thinner the dense LSM electrodes are, the smaller the resistance to ionic transport through the dense LSM layer and therefore the more active the LSM surface becomes for oxygen reduction. In particular, a characteristic thickness was defined as the thickness at which the interfacial polarization resistance drops below 1/e, or ~37%, of its peak value (corresponding to the polarization resistance of the TPBs). For dense LSM, this characteristic thickness was found to be 0.36 μm at 700°C. Much greater than 0.36 μm in thickness, ionic diffusion is sufficiently difficult such that oxygen ion transport through the LSM electrode is essentially negligible. Beyond this point the surface of LSM electrodes cannot be effectively used and the behavior of the electrode is determined largely by the TPBs of the electrodes. As expected, the characteristic thickness of an MIEC electrode varies with temperature.

For very thin electrodes, the sheet resistance may dramatically reduce the effective utilization of the electrode. When this happens, it may no longer be valid to assume that the entire surface area is active. Computational modeling techniques have been used to demonstrate a corresponding drop in the effective utilization of the cathode with decreasing thickness.

On one hand, the critical thickness at which the LSM surfaces become active is important to intelligent design of practical porous mixed-conducting electrodes. On the other hand, the critical thickness at which the sheet resistance becomes dominant is important to the design of patterned electrodes for fundamental studies.

Acknowledgments

This work was supported by the DOE-NETL SECA Core Technology Program under grant no. DE-FC26-02NT41572.

The Georgia Institute of Technology assisted in meeting the publication costs of this article.

References

1. A. J. McEvoy, *Solid State Ionics*, **132**, 159 (2000).
2. B. C. H. Steele, *Solid State Ionics*, **86–88**, 1223 (1996).
3. O. Yamamoto, Y. Takeda, R. Kanno, and M. Noda, *Solid State Ionics*, **22**, 241 (1987).
4. R. A. De Souza, J. A. Kilner, and J. F. Walker, *Mater. Lett.*, **43**, 43 (2000).
5. M. Liu, *J. Electrochem. Soc.*, **145**, 142 (1998).
6. M. Mogensen and S. Skaarup, *Solid State Ionics*, **86–88**, 1151 (1996).
7. M. Liu and Z. Wu, *Solid State Ionics*, **107**, 105 (1998).
8. J. Mizusaki, H. Tagawa, K. Tsuneyoshi, and A. Sawata, *J. Electrochem. Soc.*, **138**, 1867 (1991).
9. F. P. F. Van Berkel, F. H. Van Heuveln, and J. P. P. Huijsmans, *Solid State Ionics*, **72**, 240 (1994).
10. R. Radhakrishnan, A. Virkar, and S. Singhal, *J. Electrochem. Soc.*, **152**, A210 (2005).
11. M. Suzuki, H. Sasaki, S. Otoshi, A. Kajimura, N. Sugiura, and M. Ippommatsu, *J. Electrochem. Soc.*, **141**, 1928 (1994).
12. V. Brichzin, J. Fleig, H. U. Habermeier, and J. Maier, *Electrochem. Solid-State Lett.*, **3**, 403 (2000).
13. J. Fleig, *J. Power Sources*, **105**, 228 (2002).
14. F. H. Van Heuveln, H. J. M. Bouwmeester, and F. P. F. van Berkel, *J. Electrochem. Soc.*, **144**, 126 (1997).
15. E. Siebert, A. Hammouche, and M. Kleitz, *Electrochim. Acta*, **40**, 1741(11) (1995).
16. A. Endo, M. Ihara, H. Komiyama, and K. Yamada, *Solid State Ionics*, **86–88**, 1191 (1996).
17. T. Horita, K. Yamaji, N. Sakai, Y. Xiong, T. Kato, H. Yokokawa, and T. Kawada, *J. Power Sources*, **106**, 224 (2002).
18. J. Van Herle, A. J. McEvoy, and K. Ravindranathan Thampi, *Electrochim. Acta*, **41**, 1447 (1996).
19. H. Fukunaga, M. Ihara, K. Sakaki, and K. Yamada, *Solid State Ionics*, **86–88**, 1179 (1996).
20. T. Horita, K. Yamaji, N. Sakai, H. Yokokawa, and T. Kato, *J. Electrochem. Soc.*, **148**, J25 (2001).
21. T. Yammamura, H. Tagawa, T. Saito, J. Mizusaki, K. Kamitani, K. Hirano, S. Ehara, T. Takagi, Y. Hishinuma, H. Sasaki, T. Sogi, Y. Nakamura, and K. Hashimoto, *Solid State Ionics*, **70/71**, 52 (1994).
22. (a) A. Mitterdorfer and L. J. Gauckler, *Solid State Ionics*, **117**, 187 (1999); (b) A. Mitterdorfer and L. J. Gauckler, *Solid State Ionics*, **117**, 203 (1999).
23. A. Bieberle and L. J. Gauckler, *Solid State Ionics*, **135**, 337 (2000).
24. A. Bieberle, L. P. Meier, and L. J. Gauckler, *J. Electrochem. Soc.*, **148**, A646 (2001).
25. J. Fleig, *Solid State Ionics*, **161**, 279 (2003).
26. J. Fleig, J. Maier, *Solid State Ionics*, **85**, 9 (1996).
27. E. Koep, C. Compson, and M. Liu, *Solid State Ionics*, **176**, 1 (2005).
28. M. Joseph, P. Manoravi, H. Tabata, and T. Kawai, *J. Appl. Phys.*, **92**, 97 (2002).
29. Y. Yao, S. Lu, H. Chen, J. Zhai, and K. Wong, *J. Appl. Phys.*, **96**, 569 (2004).
30. A. Tiwari, A. Chug, C. Jin, D. Kumar, and J. Narayan, *Solid State Commun.*, **121**, 679 (2002).
31. E. Koep, C. Jin, M. Haluska, R. Narayan, R. Snyder, and M. Liu, *J. Appl. Phys.*, Submitted.
32. R. Das, D. Mebane, E. Koep, and M. Liu, *Solid State Ionics*, Submitted.
33. S. Skinner, *Int. J. Inorg. Mater.*, **3**, 113 (2001).